ENGINEER - Vol. LIX, No. 02, pp. [87- 97], 2026

DOI: https://doi.org/10.4038/engineer.v59i2.7751

Crack Growth Model to Evaluate the Fatigue Life of Ti-6Al-4V Medical-Grade Material

Ruminda J. Wimalasiri

Abstract: Prediction of life of a component made of a certain material would be beneficial to both the manufacturer and the user. Life prediction requires knowledge of material properties such as grain size and microstructure, as well as the stress levels induced by the maximum possible loads, particularly cyclic loads under in-vivo conditions. A mathematical model was developed to assess the lifetime of components made from Ti-6Al-4V; a medical-grade titanium alloy extensively used for implant manufacturing. Attention was given to crack initiation and growth in the microstructural short cracks and physically small cracks regions, where a significant portion of the fatigue life was accumulated. Rotary-bending experiments were conducted to assess the fatigue endurance limit of the material. The surface crack was replicated at specific stages of the life to assess its propagation and thereby the crack propagation rate was calculated. The threshold values of crack length and stress intensity factor determined in this study are in good agreement with existing literature, thereby confirming the accuracy of the results. MATLAB and Microsoft Excel were used to develop mathematical models and thereby to assess the material constants. Predicted fatigue lives were validated with the experimental results, with accuracies ranging from 0.7% to 14.5%.

Keywords: Ti-6Al-4V, Fatigue, Fracture mechanics, Life prediction

1. Introduction

Fatigue failure occurs in components subjected to cyclic or fluctuating stress at nominal stresses that are often less than the static yield strength of the material [1]. The mechanisms of fatigue crack initiation are complex and wide ranging, and it has been a problem for over 150 years and continues to be so.

The use of Ti-6Al-4V in medical industry has grown rapidly because of its superior biocompatibility and appropriate mechanical properties [2]. Manufacture of surgical implants has become the largest application of wrought Ti-6Al-4V with aerospace, nuclear and automotive applications. Due to fatigue, implants made of Ti-6Al-4V fail before the expected lifetime. As an example, hip implants are designed to be in service for at least 10 years, however, implants fail in less than 10 years, and these failures have clear evidence of fatigue failure mechanism [3][4]. So, it is vital to examine the crack propagation and life expectance characteristics of implant grade Ti-6Al-4V alloy.

The aim of this research is to investigate the characteristics affecting the fatigue life of the components made of Ti-6Al-4V. Two equations have developed based on the material characteristics to evaluate the growth of microstructural short cracks (MSC) and physically small cracks (PSC). The proposed mathematical model can be used to predict the life of the components made out Ti-6Al-4V alloy and to identify the safe working conditions.

Rotating bending fatigue experiments were conducted, using mirror-polished hourglass shaped samples, to obtain the stress (S) – life (N) data. The surface replication method was used to investigate the material crack growth rate/properties. Microstructural properties were investigated. The values of relevant material constants were calculated using S-N data and a mathematical model was developed using fracture mechanics approach to quantify the fatigue life at given stress amplitudes.

1.1. Metal Fatigue

One of the earliest studies of metal fatigue was conducted by a German mining engineer WAJ Albert in 1829 [cited in 1], where he has conducted repeated load proof tests on mine hoist chains made of iron. After a tragic railway accident in France which killed around 1500-

*Eng. (Dr.) **Ruminda J. Wimalasiri**, AMIE(SL), BTech(Hons)(Eng)(OUSL), PhD (SHU, UK),*
Senior Lecturer, Department of Mechanical Engineering, The Open University of Sri Lanka.
Email: rjwin@ou.ac.lk
https://orcid.org/0000-0001-8368-5639

1800 lives in 1842, detailed research of metal fatigue began [1].
A systematic investigation concerning fatigue was first conducted on railway axles by August Wohler [5], in 1860. Most of Wohler's work has been confirmed by Bauschinger in 1886 [Cited in 4]. Currently, three fatigue analysis approaches have been identified, the stress life approach, strain life approach and fracture mechanics approach [6].
Fatigue cracks can initiate from scratches, pits, inclusions, grain boundaries and other high stress concentrations such as sharp corners, on or near to the surface of the component. In ductile polycrystalline metals, fatigue crack initiates from a weaker grain due to reversed shear stress associated with bands of intense slip [7]. In the early stage microcracks grow on planes of maximum shear, which is known as the Stage I and after traversing several grain boundaries, the crack propagates along the planes of maximum principal stress, which is defined as Stage II as illustrated in Figure 1 [8]. Crack propagation curves are schematically shown in Figure 2 [9].

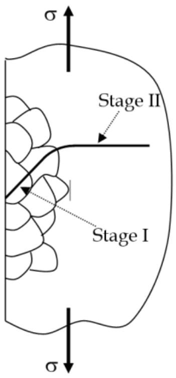

Figure 1 - Stage I and Stage II fatigue crack growth

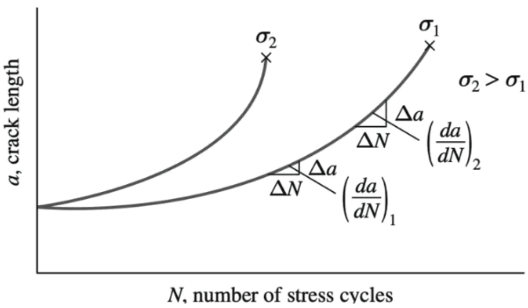

Figure 2 - Typical crack growth behaviour in constant amplitude fatigue loading [10]

1.2. Fatigue Life of Components
The general crack growth behaviour of polycrystalline metals is shown in Figure 3 [11] as a curve da/dN (crack growth rate) versus stress intensity factor range ($\Delta K = K_{max} - K_{min}$). Fatigue crack growth can be classified into three regions, namely MSC, PSC and long cracks. For stress levels around the fatigue limit, short fatigue crack growth in the MSC and PSC regimes are the most dominant regions where most of the total fatigue life is spent [12]. In the MSC regime, the size of the grains and the obstruction to crack propagation specifically grain boundaries play an important role in fatigue performance [12]. The short crack growth region represents a significant proportion of the fatigue lifetime, and its growth behaviour depends on operating stress amplitude, loading mode, environment and material properties.

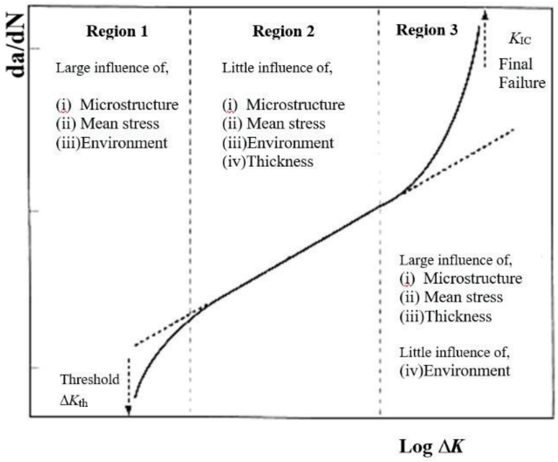

Figure 3 - Schematic illustration of crack growth [11]

Region 1 deals with low stress intensity values where crack behaviour is associated with the threshold stress intensity range (ΔK_{th}). This is the region where the cracks (MSC) propagate, and life of the component is largely dependent on the microstructural properties of the material. The literature states that these cracks do not behave according to the predictions governed by the long crack theories. Typical growth rate curves for these microstructural cracks are shown in Figure 4 [11].

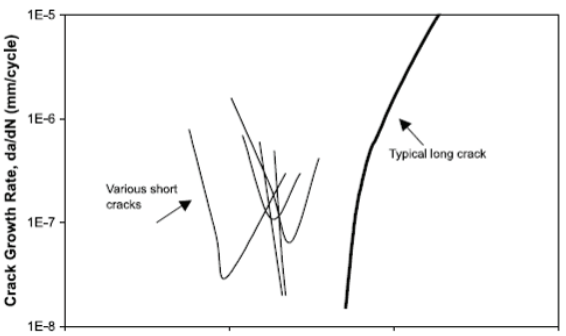

Figure 4 - Typical crack growth rate data for short cracks [11]

Figure 4 illustrates the typical properties of the microstructural cracks; where each crack begins by growing more quickly than predicted by long crack growth models and some of them actually stop growing, they simply arrest. Cracks which do not arrest come to a minimum growth rate and then speed up and eventually form long cracks. The grain boundary is a barrier to plastic deformation and therefore crack extension which is a process of plastic deformation occurs within the first grain [12].

For Stage I short crack growth, Hobson [13] proposed an equation which describes the propagation of fatigue cracks within the first grain of a polycrystalline material. The equation considers the microstructural feature in terms of a barrier to propagation and its influence on fatigue crack growth. Thus,

$$da/dN = A\ (\Delta\sigma)^m\ (d - a) \qquad \text{... (1)}$$

Where d is microstructural length parameter, A and m are material constants, a is the surface crack length and $\Delta\sigma$ is the stress range.
Crack opening mode or Mode I which relates to Stage II, the crack growth equation has been expressed by Brown et al., [14] as,

$$da/dN = B\ (\Delta\sigma)^n a - D \qquad \text{...(2)}$$

where B and n are material constants, D represents a crack growth threshold value. Hobson's equation considered mainly the crack growth rate in MSC regime which considered the microstructural features of the material, and Brown's equation considered both PSC (EPFM: Elastic Plastic Fracture Mechanics) and LEFM (Linear Elastic Fracture Mechanics) crack growth regimes.
Region 2 crack growth behaviour can be explained under LEFM by the Paris-Erdogan [15] equation,

$$\frac{da}{dN} = C(\Delta K)^m \qquad \text{... (3)}$$

This could be applied in Region 2, where C and m are material constants.
In Region 3 the crack is unstable and rapid crack growth occurs with failure at K_{IC} which is Plane Strain Fracture Toughness.
A schematic representation of crack propagation rate (da/dN) against crack length (a) is shown in Figure 5 [16]. It is evident that significant difference exists between the behaviour of short and long fatigue cracks, as determined by LEFM. It can be seen that a threshold value of ΔK_{th} exists for long cracks, below which they do not propagate. However, short cracks can grow at values of ΔK below the long crack threshold value, ΔK_{th}. It is extremely difficult to calculate stress intensity factor (K) for short cracks [17] mainly due to the change in shape function, susceptibility of short cracks to local stress fields and difficulty in measurements.

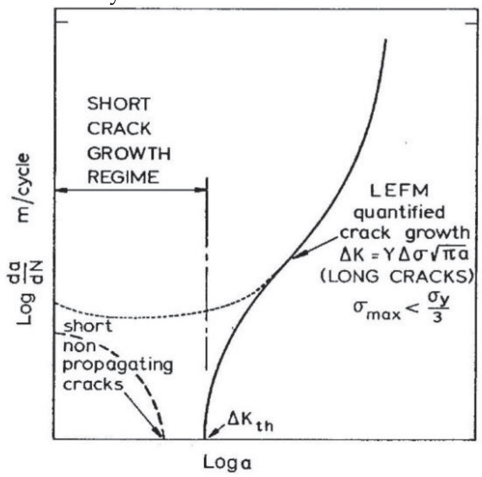

Figure 5 - A schematic illustration of *da/dN* against *a* (crack length)

Short and long crack growth models developed by Hobson [13] and Brown [14] allow the fatigue life at a given stress amplitude to be calculated. These models have been used by Angelova and Akid [17], Wheelhouse [18], Al-Alkawi [19], and Zhang [20]. However, these models were developed for different materials, not for Ti-6Al-4V medical-grade alloy.

1.3. Microstructural Effects on Fatigue Behaviour

The grain size and orientation or morphology are significant in fatigue crack initiation and growth [21]. The small cracks will grow up to a barrier such as a grain boundary and then may arrest, which depends on the microstructural characteristic dimension, d, which is material and the applied stress level dependent [16]. It is understood that materials which have fine equiaxed microstructure show higher resistance to short crack propagation [22].
Medical-grade Ti-6Al-4V is a $\alpha + \beta$ alloy with fine equiaxed microstructure. Lutjering et al. [23] showed, through comparison of average propagation rates of small surface cracks for two grain sizes, that small surface cracks propagate at a lower rate in the fine-grained material.

1.4. Fatigue Behaviour of Ti-6Al-4V Alloy

Numerous studies conducted on the crack nucleation in $\alpha + \beta$ Ti alloys have revealed that the crack initiation is due to occurrence of heterogeneous deformation in the form of intense slip bands [29]. Eylon and Pierce [31] showed in Ti-6Al-4V alloy, the portion of life attributed to crack nucleation and growth to a detectable crack size is more than 85%. Wanger and Lutjering [22] (Figure 6) have investigated the growth of short fatigue cracks in Ti-6Al-4V alloy with different microstructures which highlighted the importance of the initial size of defects to the fatigue life.

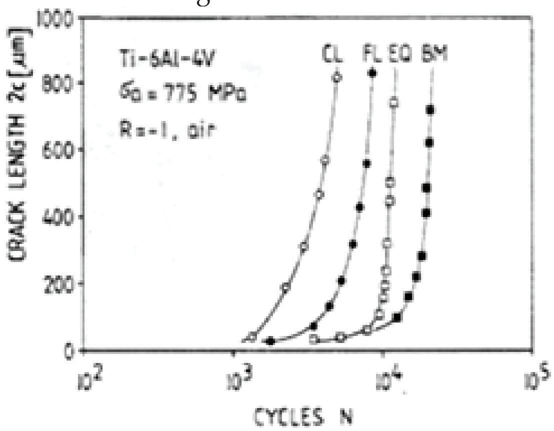

Figure 6 - Growth of short fatigue cracks of different microstructures of Ti-6Al-4V at R = -1, in air at 775 *MPa* stress amplitude: CL; coarse lamellar, FL; fine lamellar, EQ; equiaxed, BM; bi-model [22]

The observations near threshold region are very important in short fatigue crack studies. Figure 7 [32] shows experimental results of crack growth behaviour for Ti-6Al-4V alloy which shows the variation of ΔK for different microstructural arrangements and the fine equiaxed microstructure has the lowest ΔK. Research related to $(\alpha + \beta)$ titanium alloys have shown that the microstructure of the material can have an adverse effect on fatigue crack propagation and threshold behaviour for long cracks [25].

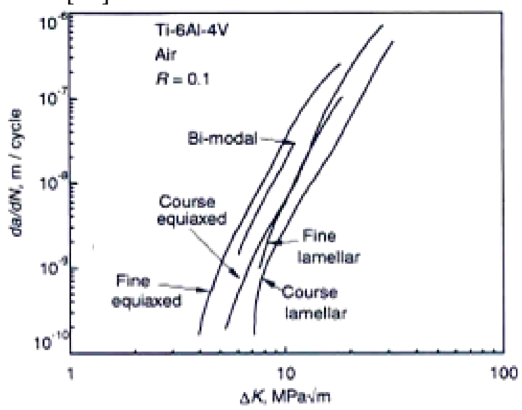

Figure 7 - Crack growth rates vs. ΔK in Ti-6Al-4V at R = 0.1 in air, fine equiaxed structure and coarse equiaxed has average α grain size of 2 μm and 12 μm [32]

Figure 8 shows the variation of fatigue crack propagation rate against the stress intensity factor range for Ti-6Al-4V alloy [22]. It was observed that crack nucleating at slip bands in the α grain and propagated along slip bands in the equiaxed microstructure, where α-grain boundaries and phase boundaries between α and β grains act as microstructural barriers to crack propagation.

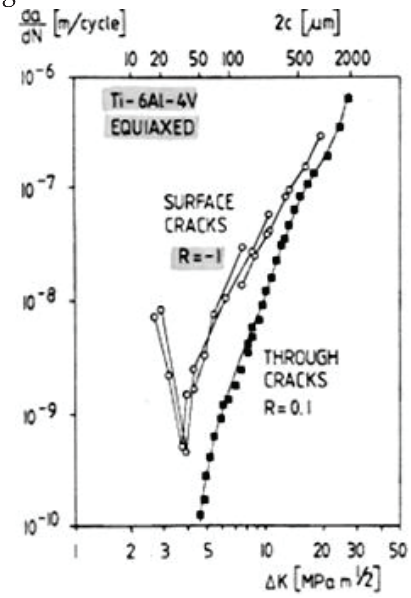

Figure 8 - Fatigue crack propagation of short surface cracks as compared to long through cracks in Ti-6Al-4V with equiaxed microstructure [22]

1.5. Microstructure and Grain Size Determination

The mirror polished samples were etched by Kroll's reagent (4*ml* HNO_3, 2*ml* HF and 94*ml* H_2O) [24] and microstructure in longitudinal and transverse directions were examined (Figure 9).

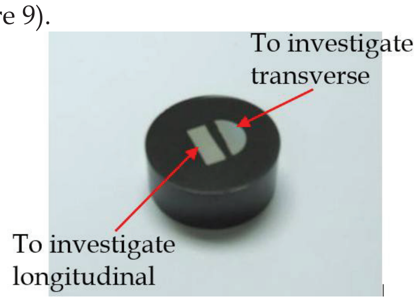

Figure 9 - Sample prepared for microstructural investigation

The average grain size was determined using mean linear intercept (MLI) method in accordance with BS 4490:1989 Section 3. In MLI method the number of grain boundaries intercepting linearly (N) for a total length of (L) were counted. The mean number of intercepts ($\bar{N}$) was determined evaluate the mean number of intercepts over the total distance, i.e. ($\bar{N}_L$).

$$\bar{N}_L = \frac{\bar{N}}{L} \qquad \dots(4)$$

The grain size $(\bar{d})$ was expressed as the mean value of the intersected segment since the material microstructure is in equiaxed state.

$$\bar{d} = \frac{1}{\bar{N}_L} \quad \ldots(5)$$

1.6. Parameters of Surface Roughness Measurement

Rz is an amplitude parameter representing the maximum peak to valley height within the sampling length, Figure 10, which is,

$$Rz = Rp + Rv$$

where *Rp* and *Rv*, are the maximum depth profile below the mean line and maximum height profile above the mean line, respectively. *Rz(max)* is considered as the surface roughness value.

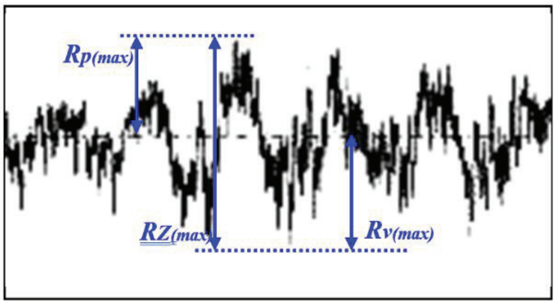

Figure 10 - Surface roughness profile and the illustration of *Rz(max)* roughness number

2. Methodology

2.1. Crack Growth Models

The crack growth model developed is based on equations (1) and (2). The fatigue crack will continue to grow if the applied stress is sufficient to overcome the microstructural barriers and then the crack grows into the PSC region finally propagating as a long crack to failure. The fatigue life spent in the MSC (*Nmsc*) and PSC (*Npsc*) regions can be obtained by integrating equation (1) and (2) respectively as,

$$N_{msc} = \frac{1}{A(\Delta\sigma)^m} \cdot ln \left[\frac{d-a_i}{d-a_{th}}\right] \quad \ldots(6)$$

and,

$$N_{psc} = \frac{1}{B(\Delta\sigma)^n} \cdot ln \left[\frac{a_{th}-(D/B(\Delta\sigma)^n)}{a_f-(D/B(\Delta\sigma)^n)}\right] \quad \ldots(7)$$

where, a_i is the initial crack length, which is the surface finish, a_{th} represents the transition length of cracks from MSC to PSC and a_f corresponds to the failure crack length.

The total lifetime (*N*) is equal to the sum of the short and long crack fatigue lifetimes.

$$N = Nmsc + Npsc \quad \ldots(8)$$

2.2. Development of Mathematical Model

Figure 11 represents a simple diagram illustrating the model. MATLAB and Microsoft Excel are used to develop the mathematical models. The constants *A*, *B*, *D*, *m*, and *n* are material-dependent and are generally determined empirically. In this work, these constants are determined using experimentally obtained S–N fatigue data and fatigue crack growth data acquired through surface replication. The determination of these constants for the MSC and PSC regimes is challenging and requires extensive mathematical iteration procedures.

The results obtained from the developed fatigue model are compared with the experimental data. Figure 12 is a schematic representation of crack growth pattern considered to develop the crack growth model. The figure shows arbitrary growth transition point (a_t) from MSC to PSC at grain 3. However, this transition point varies according to the working stress amplitude, i.e. under higher stress amplitudes PSC growth can occur at a lesser grain number.

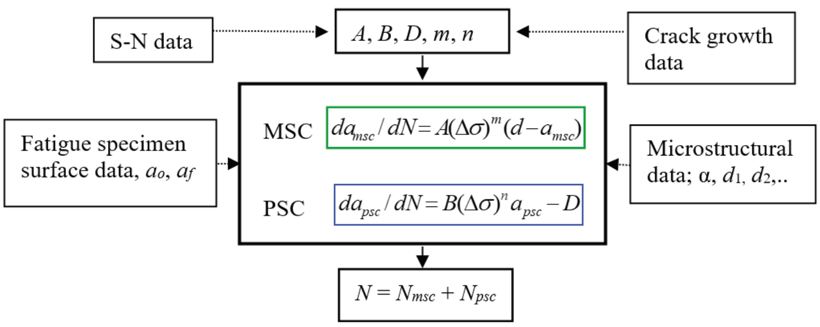

Figure 11 - Simple illustration of mathematical model

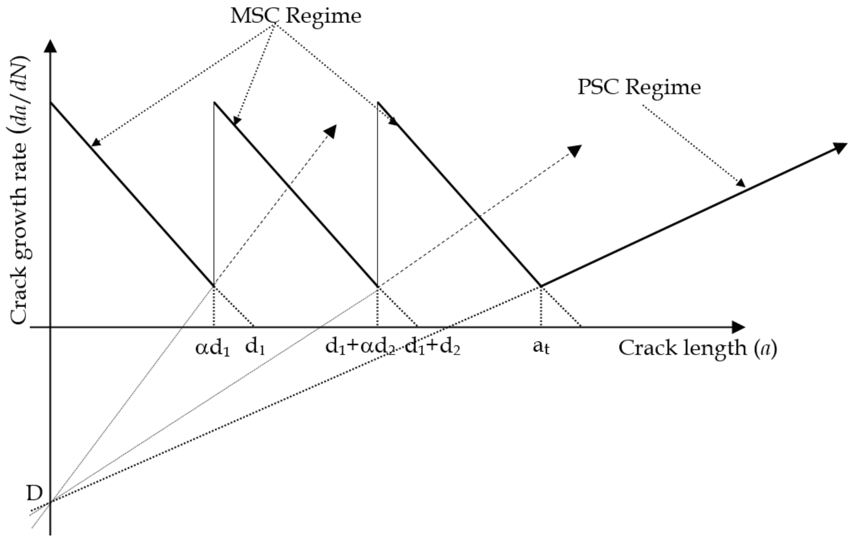

Figure 12 - Schematic diagram which represent the MSC and PSC propagation

The main steps of model development are:

Step.1. Considering equation (1) and (2), crack rates of MSC $\left(\frac{da_{msc}}{dN}\right)$ and PSC $\left(\frac{da_{psc}}{dN}\right)$growths were calculated.

Step.2. The transition number of grains was calculated according to crack growth values.

Step.3. The value of a_t was calculated.

Step.4. The number of cycles sustained in MSC (*Nmsc*) and PSC (*Npsc*) regimes were calculated for different stress amplitudes according to the transition point (a_t) determined under step.3.

Step.5. Calculated the total number of cycles ($N = Nmsc + Npsc$) sustained before failure.

3. Results and Discussion

3.1. Grain Size Determination

The microstructure of the Ti-6Al-4V alloy is shown in Figure 13. The MLI method in accordance with BS 4490:1989 Section 3 was followed, and the grain size is calculated as 7 μm. The microstructure is in accordance with plate A1 of the ETTC Publication 2 and complies with BS 7252-Part 3 (1997).

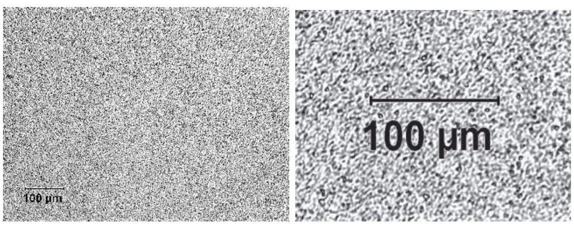

Figure 13 - Microstructure of implant grade wrought Ti-6Al-4V alloy in transverse direction

3.2. Surface Roughness Measurements

A Taylor-Hobson Talysurf-120L, stylus type apparatus with a 2 μm stylus tip radius, was used. Measurements were taken over a nominal 5 mm length using 0.8 mm cut off filter. Four readings were taken along the longitudinal direction around the sample at 90^{o} angular intervals as shown in Figure 14 and these positions are numbered as 1, 2, 3 (on the other side) and 4. The maximum *Rz* is 0.2 μm.

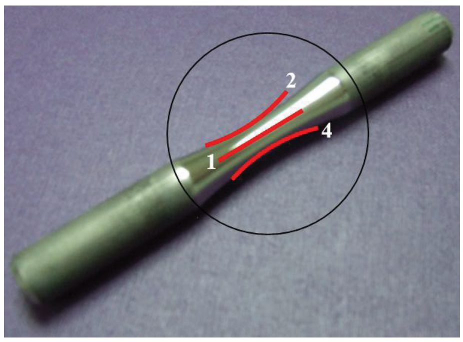

Figure 14 - Test specimen and locations at which surface roughness measurements were taken

A typical surface profile of a machined sample obtained from the Talysurf is shown in Figure 15.

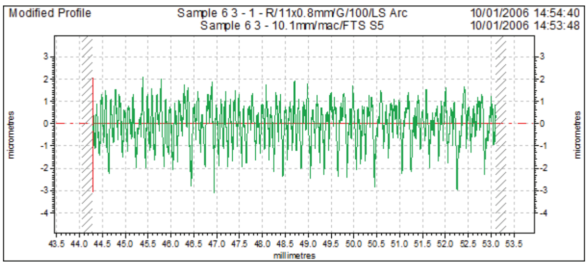

Figure 15 – Typical surface profile of a machined sample obtained from Talysurf

The surface roughness was noted as three measuring parameters, namely *Ra* - average roughness, *Rp(max)* - maximum peak height and *Rv(max)*- maximum valley depth.

3.3. Analysis of Fatigue Cracks using a Surface Replication Technique

The surface replication technique, employing acetate films and acetone, was used to evaluate the crack propagation behaviour in Ti-6Al-4V. Small strips of acetate paper were used for surface replication. Drops of acetone were applied to soften the acetate, allowing it to adhere to the specimen surface. After drying, the acetate film was carefully removed and examined under a microscope. Once a crack was detected, the same area was repeatedly replicated at specified cycle intervals. Crack propagation was then measured at the required time intervals (i.e., number of cycles). Mirror-like polished samples with a surface roughness of 0.2 *μm* were used in this investigation. Samples were tested at stress amplitude of 630 *MPa*, where the fatigue endurance limit of a batch of similar samples is 595 *MPa*. Where cracks were found, pictures were taken at increasing number of cyclic intervals, which are shown in Figure 16. The fraction of the life (N/N_f) at each interval is noted on the figure.

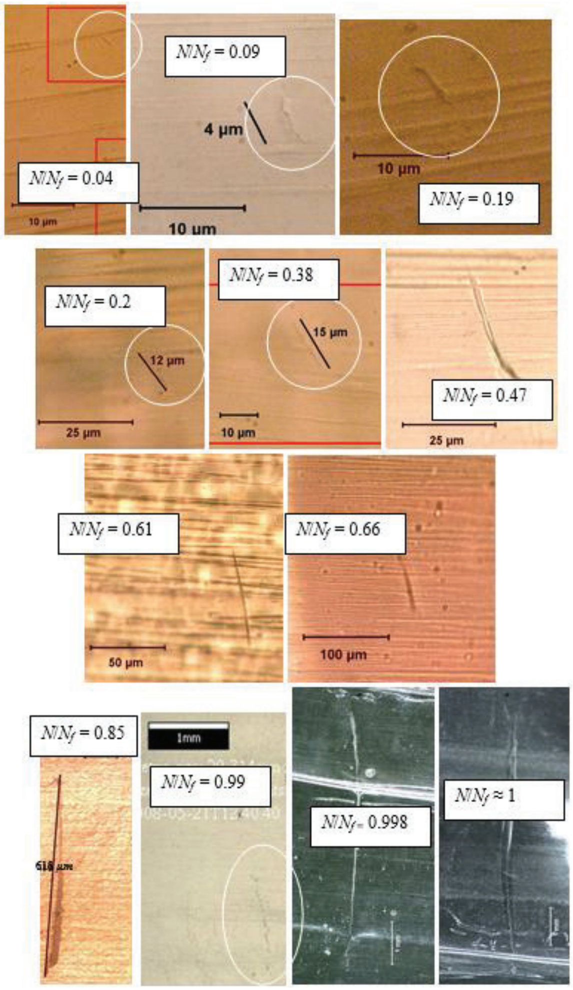

Figure 16 - Pictures of fatigue cracks obtained by surface replication

No. of Cycles	Crack length (μm)
10000	2
20000	4
40000	5
50000	7
80000	12
90000	15
100000	21
110000	40
130000	57
140000	90
150000	*150*
160000	240
170000	*334*
180000	619
200000	*1200*
209267	6360
209487	*6700*
209873	10450

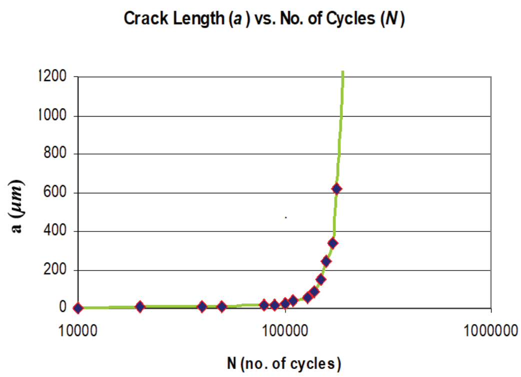

Figure 17 - Crack length against the number of cycles

The variation of *a* with the increment of *N* is shown in Figure 17. Based on the crack length measurements fatigue crack growth rate (*da/dN*) against the crack length (*a*) can be determined, as shown in Figure 18. It can be noted that there is a reduction of crack growth when the crack length approaches a crack length of around 7-8 *μm*. Based on the *a* versus *N* data and applied stress, the fatigue crack growth rate (*da/dN*) against stress intensity factor (ΔK) curve can be determined, as shown in Figure 19. According to the figure it can be noted that there is a threshold value of the stress intensity factor around 3-5 $MPa\sqrt{m}$.

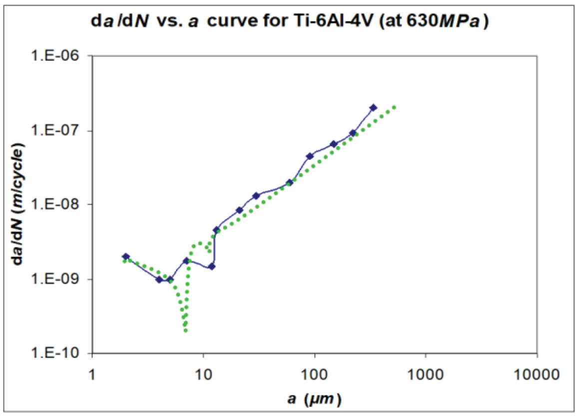

Figure 18 - Variation of fatigue crack growth rate (*da/dN*) against the crack length (*a*)

This compares favourably with literature values of around 5 $MPa\sqrt{m}$ [25][22]. The respective values of ΔK corresponding to cracks lengths were calculated using LEFM equation, $\Delta K_{th} = Y\Delta\sigma_{th}\sqrt{\pi a}$. The value of the geometrical factor, Y, is approximated as unity [26][27][28].

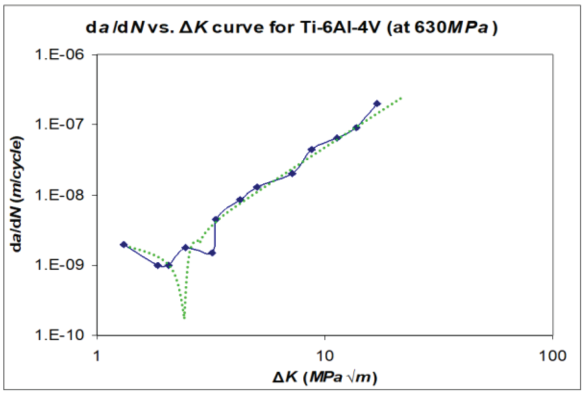

Figure 19 - Variation of *da/dN* against *ΔK*

Determination of parameter *d*: The parameter d represents the crack length where crack growth rate decreases to a minimum, and cracks tend to slow down and may arrest. This corresponds to a position where the crack front meets the main microstructural barrier such as a grain boundary. For this model the value of d was taken as the α-grain size of the material, since the α-grains are the sites for micro-crack nucleation, and Stage I crack growth [29][30] in Ti-6Al-4V alloy. The mean grain size is taken as 7 μm. The da/dN vs. a curve obtained from the data obtained from surface replication (Figure 18) also supports the existence a barrier at ≈ 7 μm.

Determination of Parameter a_i: The parameter a_i is the initial defect size where fatigue failure nucleates. It is considered as the surface finish (initial defect size) of the smooth specimens (highly polished samples to mirror surface finish). The surface finished to 0.2 μm is considered as a_i value.

Determination of Parameter a_f: The parameter a_f represents the final crack length and this is taken to be half of the minimum diameter of the test specimens which is 4000 μm (= 8/2 mm).

Determination of Parameter a_t: The transition crack length can be calculated using equations (1) and (2), which the crack growth rates of both MSC and PSC should be equal, i.e.,

$$\frac{da_{msc}}{dN} = \frac{da_{psc}}{dN},$$

which can be expanded as:

$$a_t = \frac{A(\Delta\sigma)^m[d_1+(t.grain-1)\ d_2]+D}{A(\Delta\sigma)^m+B(\Delta\sigma)^n} \qquad \ldots(9)$$

where, t.grain is the grain number which the crack transfer from MSC to PSC and it is considered as $d_1 = d_2 = d_3$ ......= 7 μm for the model.

Determination of Parameter *D*: The parameter D is a material constant. Considering equation (2) the value of D can be expressed as $D = B(\Delta\sigma)^n a_{th}$. Explaining further, the value of D is the intercept of da/dN vs. a curve (PSC region which is governed by the equation 2), as shown in Figure 20.

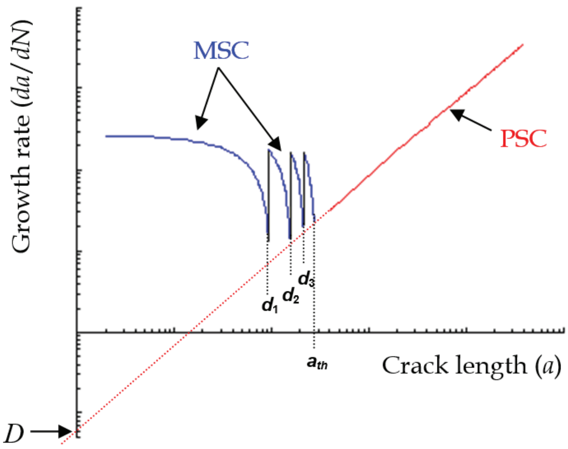

Figure 20 - Typical *da/dN* vs. *a* representation of fatigue cracks in MSC and PSC regions

The value of D is calculated by the fatigue crack growth data in PSC regime (a > 40 μm) obtained by surface replication, which are given in Figure 16. The da/dN vs. a curve can be obtained as shown in Figure 21 and the value of D (interception of Y-axis) can be calculated as 3.99 x 10^{-3}.

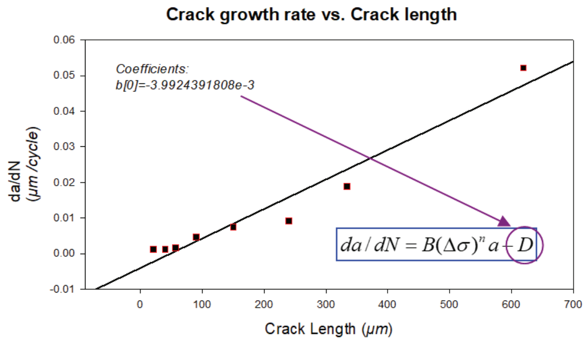

Figure 21 - *da/dN* vs. *a* curve for PSC regime obtained using surface replication data, to determine the value of parameter *D*

The model assumes a crack retardation threshold condition at the crack arrest ($da/dN \rightarrow 0$) due to existence of a plastic slip zone ahead of crack front in MSC growth. If r_p is the extent of crack front plastic zone size, a_{msc} and d can be represented as shown in Figure 22. The plastic zone size is constrained by the grain boundaries which the cracks propagate into the next grains.

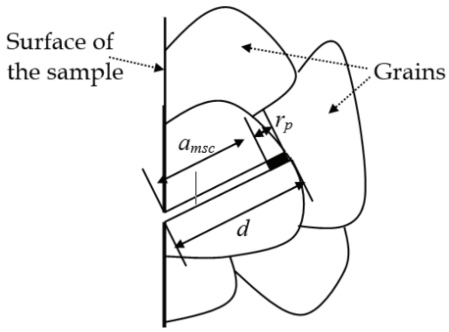

Figure 22 - Schematic illustration of the crack tip plastic zone in MSC

The a_{msc} can be represented as [18][20],

$$a_{msc} = \alpha \cdot d \qquad \ldots(10)$$

The value α depends on the microstructure of the material, which can be represent as,

$$\alpha = 1 - \left({r_p}/{d}\right) \qquad \ldots(11)$$

The value of α is taken as 0.95, consistent with values used in similar models. [18][20].

4. Results Summery

The material constants were determined by theoretical analysis using the computer models developed by Matlab and Microsoft Excel. The values given are the best fit values for the experimental S-N data obtained from smooth specimen rotary bending fatigue tests.

$A = 8.9 \times 10^{-7}$
$B = 6.585 \times 10^{-27}$
$D = 3.99 \times 10^{-3}$
$m = 1.01$
$n = 7.854$

The MSC and PSC fatigue crack growth equations for Ti-6Al-4V alloy are derived as,

MSC growth:

$$\frac{da}{dN} = 8.9 \times 10^{-7} (\Delta\sigma)^{1.01} (d - a)$$

PSC growth:

$$\frac{da}{dN} = 6.585 \times 10^{-27} (\Delta\sigma)^{7.854} a - 3.99 \times 10^{-3}$$

Units of the parameters are, da/dN in $\mu m/cycle$, $\Delta\sigma$ in MPa, a and d in μm.

4.1. Lifetime Predictions for Ti-6Al-4V

Four separate tests we conducted to check the accuracy of the proposed mathematical equation. A comparison of experimental results obtained by smooth specimen fatigue tests, with the results obtained from the equations, is tabulated in Table 1 and illustrated in Figure 23.

Table 1 - Comparison of experimental results obtained by smooth specimens with the results obtained from the model

Specimen	Stress Amplitude (MPa)	Fatigue Life (Experimental) (No. of Cycles)	Fatigue Life (Model) (No. of Cycles)	% Variation
1	690	54610	54992	0.7
2	612	136981	117078	14.5
3	699	47820	51336	7.3
4	650	79975	83485	4.4

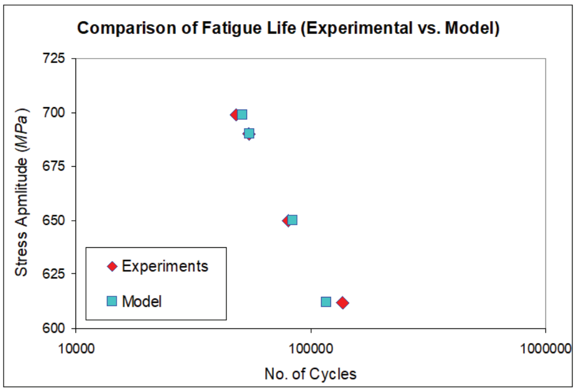

Figure 23 - Lifetime predictions, experimental results obtained by smooth specimens vs. the model

The comparison shown in Table 1 and Figure 23 suggests that the crack propagation model successfully predicts the fatigue life of the smooth specimen for constant amplitude loading for the limited number of points available to this comparison. The accuracy (variation) of the predictions is from 0.7% to 14.5%.

4. Conclusions

The microstructural analysis shows that the average grain size of the selected implant grade Ti-6Al-4V material is 7 μm. Based on the results obtained by analysis of surface cracks by replication, it can be concluded that, at the $\Delta\sigma_{th}$ = 630 *MPa*, an existence of microstructural barrier ≈ 7-8 μm. The relative threshold stress intensity factor at this dimension is 3-5 $MPa\sqrt{m}$.
Based on two existing models for MSC and PSC regimes, mathematical models to predict the crack growth rate for Ti-6Al-4V implant grade alloy for both the regimes were developed as,

MSC growth:

$$\frac{da}{dN} = 8.9\times10^{-7}(\Delta\sigma)^{1.01}(d-a)$$

PSC growth:

$$\frac{da}{dN} = 6.585\times10^{-27}(\Delta\sigma)^{7.854}a - 3.99\times10^{-3}$$

The total lifetime (N) is equal to the sum of the short and long crack fatigue lifetimes, i.e.

$$N = N_{msc} + N_{psc}$$

$$N = \frac{1}{A(\Delta\sigma)^m}\cdot ln\left[\frac{d-a_i}{d-a_{th}}\right] + \frac{1}{B(\Delta\sigma)^n}\cdot ln\left[\frac{a_{th}-(D/B(\Delta\sigma)^n)}{a_f-(D/B(\Delta\sigma)^n)}\right]$$

The predicted fatigue lifetime of Ti-6Al-4V implant grade alloy is validated for 4 different stress amplitude which shows an accuracy of the 0.7% to 14.5%. The accuracy of the proposed equation can be further justified by comparing with more fatigue experimental results.

Acknowledgement

Author wishes to acknowledge the immense guidance given by Dr. Upul S. Fernando, Prof. Robert Akid and Dr. Anita Clark.

References

1. Suresh, S., Fatigue of Materials, Cambridge Solid State Science Series, Cambridge University Press, 1991, ISBN 0 521 36510 4.
2. Brunette, D. M., Tengvall, P., Textor, M., Thomson, P., Titanium in Medicine, Sringer, *Springer-Verlag Berlin Heidelberg*, 2001; ISBN 3-540-66936-1.
3. Organ-Hough, C. V. J., Tavakkolizadeh, A., Case Report, Fatigue Failure of the Femoral Component of a Cementless Total Hip Arthroplastry, *The Journal of Arthroplasty*, 2004; vol. 19, No. 5, p. 658-60.
4. Sharma Dinesh, K., Stuart Brooks., Stuart Creasey., Brian Lewis., Fracture of fully hydroxyapatite-coated titanium femoral stem of a total hip replacement-a report of 3 cases, *Acta Orthop Scand*, 2004; 75 (6), p 768-71.
5. Wohler, A., (1860), Versuche uber die festigkeit dev eisenbahnwagenachsen, Seitschrift fur Bauwesen 10; English Summary (1867), *Engineering*, 4, 160-1.
6. Julie A. Bannatine., Jess J. Comer., James L. Handrock., Fundamentals of Metal Fatigue Analysis, Prentice Hall, Englewood Cliffs, New Jersey 07632, ISBN 0-13-340191-X.
7. Brown, L. M., Ogin, S. L., (1985). Role of Internal Stress in the Nucleation of Fatigue Cracks. In B. A. Bilby, K.J. Miller, & J.R. Willis (Eds.), Fundamentals of Deformation and Fracture: *Eshelby Memorial Symposium* (pp. 501–528). Cambridge University Press.
8. Brown, M. W., Interface between short, long, and non-propagating cracks, EGF Pub.1 (edited by Miller KJ, de los Rios ER), 1986, Mechanical Engineering Publications Ltd, London, 1986, pp 423-39.
9. Suresh, S., Fatigue of Materials, 2nd Edition, University of Cambridge, Cambridge, 1998; ISBN 0-521-57847-7.
10. Sundar., (2022, February 9). What is the Fatigue Crack Propagation Rate. https://extrudesign.com/what-is-the-fatigue-crack-propagation-rate/. (Referred in 2025 December 9).
11. Mughrabi, H., Microscopic Mechanisms of Metal Fatigue, Strength of Metals and Alloys (Edited by

P. Haasen, V. Gerold, and G. Kostorz), 1980; vol. III (Pergamon, Oxford) p. 1615-38

12. Taylor David., Modelling of Fatigue Crack Growth at the Microstructural Level, *Computational Materials Science*, 25 (2002) 228-236.

13. Hobson, P. D., (1985), The Growth of Short Fatigue Cracks in a Medium Carbon Steel, Ph.D Thesis, University of Sheffield, Sheffield.

14. Brown, M.W., Miller, K. J., Fernando, U. S., Yates, J. R., Suker, D. K., Aspects of multiaxial fatigue crack propagation, *Fourth International Conference on Biaxial/Multiaxial Fatigue*, May 31-June 03, 1994, Paris, France.

15. Paris, P. C., Erdogan, F., (1963), A critical analysis of crack growth propagation laws, *Journal of Basic Engineering*, 85, 528-34.

16. Miller, K. J., The Propagation Behaviour of Short Fatigue Cracks, Department of Mechanical Engineering, University of Sheffield, Sheffield, 1987.

17. Angelova, D., Akid, R., A note on modelling short fatigue crack behaviour, *Fatigue and Fracture of Engineering Materials and Structures*, 1998, 21, 771-779.

18. Wheelhouse, K., Fatigue Damage Accumulation Under Torsion and Non-proportional Push-pull Interruption Loading, PhD thesis, Sheffield Hallam University, 2002.

19. Al-Alkawi, H. J. M., Cumulative Fatigue Damage Under Varying Stress Range Conditions, PhD thesis, University of Sheffield, 1986.

20. Zhang, W., Short Fatigue Crack Behaviour Under Different Loading Conditions, PhD thesis, University of Sheffield, 1991.

21. Ohchang, Jin., Richard, W., Hamm, W., Steven Johnson., Microstructural influences on the growth of small cracks in Ti-6Al-4V, 2002 Blackwell Science Ltd, *Fatigue Frac EngngMater Struct*, 25, 563-574.

22. Lothar Wanger., Gerd Lutjering., Microstructural Influence on Propagation Behaviour of Short Cracks in an (α+β) Ti Alloy, *Zeitschrift fur metallkunde*, 1987; 78, 5, p. 369-75.

23. Lutjering, G., Gysler, A., Wanger, L., *Proc Sixth world conference on Titanium*, Paris, France 1988.

24. Voort, G. F. V., Microstructure of titanium and its alloys, *Industrial Heating* [0019-8374], 2006, vol:73, iss:8, pg:77 -84.

25. Brown, C. W., Smith, G. C., The Effect of Microstructure and Texture on the fatigue Crack Growth Threshold in Ti-6Al-4V, *Intergovernmental Conference-EU*, 1982, Vol 1, 329-343.

26. Kruzic, J. J., Ritchie, R. O., Technical Note; Kitagawa-Takahashi Diagrams Define the Limiting Conditions for Cyclic Fatigue in Human Dentin, Published online 29 September 2006 in Wiley Inter Science (www.interscience.wiley.com).

    DOI: 10.1002/jbm.a.30939.

27. Hudak, S. J. Jr., Small crack behaviour and the prediction of fatigue life, *Transaction of the ASME*, 26, Vol.103, January 1981.

28. Monty A. Moshier., Theodore Nicholas., Ben M. Hillberry., High Cycle Fatigue Threshold in the Presence of Naturally Initiated Small Surface Cracks, *ASTM special publications*, 2002, 1417, 129-146.

29. Nakajima, K., Terao, K., Miyata, T., The effect of microstructure on fatigue crack propagation of α+β titanium alloys- in-situ observation on short fatigue crack growth, *Material Science and Engineering*, 1998; A243, P. 176-81.

30. Benson, D. K., Grosskreutz, J. C., Shaw, G. G., Mechanisms of fatigue in mill annealed Ti-6Al-4V at room temperature and 600°F, *Metal transactions*, 1972; vol. 3, issue 5, P. 1239-48.

31. Eylon, D., Pierce, C. M., Effect of microstructure on notch fatigue properties of Ti-6Al-4V, *Metallurgical Transactions*, 1972; vol. 7, issue 1, p. 111-21.

32. Rodney Boyer., Gerhard Welsch., Collongs E. W., Materials Properties Handbook: Titanium Alloys, ASM International, 1994; ISBN 0-87170-481-1.